Development of an Aeroacoustic Prediction Tool for Wind Turbine Noise

João Henrique Souto
joaohenriquesouto@tecnico.ulisboa.pt

Instituto Superior Técnico, Universidade de Lisboa, Portugal

July 2017

Abstract

From all the renewable sources of energy, wind energy is among the ones with a more rapid development. With this rapid deployment of wind turbines, so does the impact of wind turbines grow, leading to an increase in the awareness about these impacts on the environment and human health. A considerable part of the research has focused on the noise impact of wind turbines, improving the performance of the turbines in the process. The objective of this work was to create a modular software, that could be used to predict the noise produced by different blade geometries, allowing the user to define new blades, with different number of sections and panels, airfoil profiles and geometric characteristics, namely twist angle. In this work, a blade element momentum theory model is implemented to predict the aerodynamic performance of wind turbines, coupled with the panel code XFOIL for automation of the procedure and blade geometry discretization. Two aeroacoustic prediction models were then employed, a semi-empirical model, based on the works of Brooks et al and Amiet, and a theoretical model, Formulation 1A of Farassat. The semi-empirical model was validated against measurement data of the NREL Phase II and AOC 15/50 wind turbines, while Formulation 1A of Farassat was verified against a validated tool used by TU Delft. The software aeroacoustic capabilities are presented at the end of the work, with an example of the type of results that can be achieved with the proper inputs.

Keywords: WT aerodynamics, Wind turbine aeroacoustics, Formulation 1A

1. Introduction

From all the renewable sources of energy, wind energy is among the ones with a more rapid development. As the technology is developed and reaches a more mature state, wind power becomes more and more accessible, to the state that it becomes competitive with more traditional sources of energy, such as fossil fuels.

Despite wind energy's growing importance, there are several negative consequences of the implantation of wind turbines (WTs). These vary from impact on the environment, namely on birds and bats, to direct impact on people's lives, particularly to those that live nearby wind turbines and are annoyed by their noise and visual impact on the landscape.

Wind Turbine noise prediction models can be divided in two types, semi-empirical correlations and theoretical models, derived from fundamental aerodynamic and aeroacoustic formulations. Semi-empirical correlations are mostly used to compute 1/3 octave bands noise, using formulas derived from aerodynamics, experiments and fittings.

On the other hand, Farassat's 1A formulation belongs to the theoretical model category. This formulation is derived from Ffowcs Williams-Hawkings' Equation [1], which in turn, is based on Lighthill's acoustic analogy [2]. Although the evolution of computational power has led to a great development of previously untapped techniques, Computational Aeroacoustics (CAA) is an area of interest that has been slow in becoming of broad use. This is mainly because of its intrinsic complexity, given the involvement of several disciplines which are still in frank expansion. Such areas, exemplified by Computational Fluid Dynamics (CFD), form the bases of CAA.

2. Wind Turbine Noise

Sound is defined as a pressure oscillation propagating through a medium. The sound pressure level (SPL) has decibel units (dB) and is defined as:

$$SPL = 10\ \log_{10}\left(\frac{p_{\text{rms}}^2}{p_{\text{ref}}^2}\right) = 20\ \log_{10}\left(\frac{p_{\text{rms}}}{p_{\text{ref}}}\right), \quad (1)$$

where p_{ref} is the reference pressure, representing the

minimum value of pressure to which the human auditory system is capable of perceiving and p_{rms} is the root mean square value of the pressure oscillation (p_{ref} is usually assumed to be $2 \times 10^{-5} Pa$ in air).

Sources of Noise

Wind Turbine noise can be of two distinct origins: Mechanical and Aerodynamic [3, 4]. Mechanical sources of sound are generally negligible in most modern WTs and will only be summarized here. These noise sources include: Gearboxes; Generator; Yaw Drives; Cooling Fans.

Sound of aerodynamic origin dominates the noise spectrum of a modern WT. Aerodynamic noise can generally be divided into narrowband (discrete-harmonics) and broadband components. The discrete-frequency noise contains the deterministic components of the thickness and loading noise, as well as the blade passing frequency (BPF) and multiple integers. Broadband noise arises from the interaction of the rotating blades and tower with the inflow, usually turbulent in nature. The following figure (Figure 1) shows the different phenomena behind the emission of noise by a moving blade.

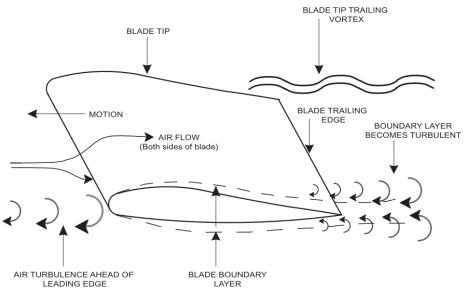

Figure 1: Aerodynamic noise sources associated with wind turbine blade (Source: [3])

Wind turbines' aerodynamic noise can generally be divided in different categories:

- Turbulent Inflow Noise;
- Turbulent Boundary Layer Trailing Edge Noise;
- Separated Stall Noise;
- Trailing Edge Bluntness Vortex Shedding Noise;
- Laminar Boundary Layer Vortex Shedding Noise;
- Tip Vortex Noise.

Formulation 1A of Farassat leads to a different division of noise terms, which result from the solution of two wave equations (Equations 3, 4). These equations yield the Loading and Thickness noise. Thickness and Loading Noise are known together as rotational noise and represent the results from linear aeroacoustic theory. Thickness noise represents the noise generated by the fluid that is displaced by the blades (displacement that is proportional to the thickness of the blade) while Loading Noise represents the noise generated due to the aerodynamic load acting on the blade.

Formulation 1A of Farassat

Formulation 1A follows Formulation 1 of Farassat, that contrary to Formulation 1A, has an observer time derivative that is taken numerically and that increases computational effort and reduces accuracy. Formulation 1A of Farassat appeared for the first time in [5]. Both Formulations are derived from Ffowcs William-Hawking (FW-H) equation, which is based on Lighthill's acoustic analogy, being an exact rearrangement of the continuity equation and the Navier-Stokes equations into the form of an inhomogeneous wave equation. The FW-H equation for an impermeable surface is given by:

$$\begin{aligned} \bar{\Box}^2 p'(\vec{x},t) &= \frac{\partial}{\partial t}\left[\rho_o v_n \delta(f)\right] - \frac{\partial}{\partial x_i}\left[P_{ij} n_j \delta(f)\right] \\ &\quad + \frac{\partial^2}{\partial x_i \partial x_j}\left[H(f) T_{ij}\right]. \end{aligned} \tag{2}$$

The symbol $\Box^2 = \frac{1}{c^2}\frac{\partial^2}{\partial t^2} - \nabla^2$ is the wave or D'Alembertian operator in 3D space and $T_{ij} = \rho u_i u_j + P_{ij} - c^2(\rho - \rho_0)\delta_{ij}$ represents the Lighthill stress tensor. $H(f)$ represents the Heaviside function, δ_{ij} is the Kronecker delta.

In the previous equation, one can see the appearance of the thickness and loading noise source terms, respectively:

$$\Box^2 p'_T = \frac{\partial}{\partial t}\left[\rho_o v_n \delta(f)\right], \tag{3}$$

$$\Box^2 p'_L = -\frac{\partial}{\partial x_i}\left[P_{ij} n_j \delta(f)\right], \tag{4}$$

where p'_T, p'_L represent the pressure perturbation due to the thickness and loading noise sources, respectively. Therefore, we want the solution of these wave equations, which in Formulation 1A of Farassat are given by:

$$
\begin{aligned}
4\pi p'_L(\vec{x},t) &= \int_{f=0}\left[\frac{\dot{p}\cos\theta}{cr(1-M_r)^2}\right]_{\text{ret}} dS \\
&+ \int_{f=0}\left[\frac{\hat{r_i}\dot{M_i}p\cos\theta}{cr(1-M_r)^3}\right]_{\text{ret}} dS \\
&+ \int_{f=0}\left[\frac{p\cos\theta(1-M_i n_i)}{r^2(1-M_r)^2}\right]_{\text{ret}} dS \\
&+ \int_{f=0}\left[\frac{(M_r-M^2)p\cos\theta}{r^2(1-M_r)^3}\right]_{\text{ret}} dS,
\end{aligned} \tag{5}
$$

$$
\begin{aligned}
4\pi p'_T(\vec{x},t) &= \int_{f=0}\left[\frac{\rho_0\dot{v_n}}{r(1-M_r)^2}\right]_{\text{ret}} dS \\
&+ \int_{f=0}\left[\frac{\rho_o v_n\dot{M_r}}{r(1-M_r)^3}\right]_{\text{ret}} dS \\
&+ \int_{f=0}\left[\frac{\rho_o v_n c M_r}{r^2(1-M_r)^3}\right]_{\text{ret}} dS \\
&- \int_{f=0}\left[\frac{\rho_o v_n c M^2}{r^2(1-M_r)^3}\right]_{\text{ret}} dS.
\end{aligned} \tag{6}
$$

Given the formulation to be used in predicting WT noise, it is then necessary to select a numerical algorithm to calculate the relevant acoustic integrals. Since Formulation 1A of Farassat is a retarded-time formulation there are some different options when considering which numerical integration algorithm to choose from.

Retarded-time formulations can be divided into two basic types:

- Observer time-dominant algorithm
- Source time-dominant algorithm

Observer time-dominant algorithm is based on using a time referential that focus on the observer. As the name implies, this approach regards the observer time as the dominant one. Consists of selecting an observer time and determining to which retarded time instant the sound emission corresponds, and then, discovering the positions of that sound source in space. This method has the disadvantage of leading to unequally spaced emission times, and therefore requires an algorithm to discover the position of the sound sources in the "past".

Source time-dominant algorithm is based on the opposite principle. As the name implies, this approach regards the source time as the dominant one. Instead of selecting an observer time and determining to which retarded time instant the sound emission corresponds, one can select the source time for each panel and verify when the sound emitted from that panel will reach the observer. In the cases of interest for WTs, the observer is immobile and therefore the observer time can be easily computed by $t = \tau + r_i/c$. This method has the disadvantage that leads to unequally spaced observer times, and therefore requires an interpolation algorithm so that the sound emitted by different panels can be added together at a certain observer time.

This algorithm presents several advantages in comparison with observer time-dominant algorithms, since it is computationally easier to know the position of a sound source, at each instant in time on this time referential and then finding at which time instant the sound emitted by that section reaches the observer than, knowing the time at which the sound reaches the observer and finding the position of that sound source in the past. Additionally, when the input aerodynamic data are obtained with CFD or even experimental methods, these data are usually written in the source time referential and therefore the use of a source time-dominant algorithm does not implicate an interpolation of the data.

A source time-dominant algorithm was used in the implementation of Formulation 1A of Farassat. Furthermore, the mid-panel formulation will be used, since aerodynamic data are usually given together with a panel discretization of the body surface, along with the pressure being applied on each panel's center.

Semi-Empirical Models

To complement the noise results that one can obtain with Formulation 1A of Farassat, and in cases where detailed aerodynamic data is not readily available, the semi-empirical models are of great use. Since the primary objective of this dissertation was not the implementation of these models, which has already been extensively done by fellow students [6], the introduction of these models was based on the work developed by Simão Rodrigues for his Master's Thesis and posterior work as a PhD Student at IST. For this, the noise calculation functions, developed by Simão in C++, were adapted to fit the code implemented, namely the interaction between BEM and XFOIL developed. This makes for a more comprehensive software, which allows for the possibility of using 2 different methods for the computation of WT noise. One method, based on a retarded time formulation (Farassat 1A), which directly yields

time dependent noise results and a different one (Semi-Empirical Models), which yield frequency dependent results.

3. Wind Turbine Aerodynamics

The dynamics behind the energy extraction process that occurs in WTs can be idealized through the actuator disc concept, where the rotor of a WT is represented by an ideal actuator disc, as presented in Figure 2. In this model it is assumed that only the mass of air that passes through the turbine's rotor is affected and that it remains separate from the surrounding air, which means that a stream-tube of circular cross section can be idealized, pertaining to the affected mass of air.

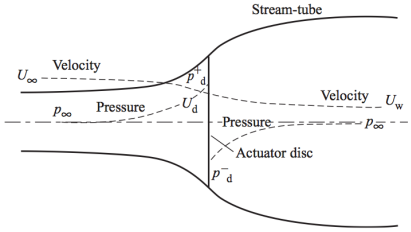

Figure 2: Actuator Disc Concept (Source: [7])

In this concept the following assumptions are made:

- The flow is considered to be steady, inviscid, irrotational, incompressible and isentropic;
- The flow is unidimensional;
- Loading and velocity are uniform over the disk area.

Over the rotor, the actuator disc models the wind energy extraction that occurs when a WT is working. The power coefficient C_P and the thrust coefficient C_T are given as:

$$\begin{aligned} C_P &= \frac{P}{\frac{1}{2}\rho U_\infty^3 A_d} = 4a\left(1-a\right)^2, \\ C_T &= \frac{P}{\frac{1}{2}\rho U_\infty^2 A_d} = 4a\left(1-a\right). \end{aligned} \tag{7}$$

Although more complex models can be used to study the airflow around a rotor, the use of BEM theory as a first approach is still common practise today, given its speed and simplicity. BEM theory results from the combination of the blade element and momentum theory. Blade element theory conceptualizes the blade as elements, where aerodynamic forces act while momentum theory follows from the actuator disc concept and discretizes the rotor actuator disc as annuli, where the momentum change occurs.

Blade element theory conceptualizes a blade in several independent elements, sections that act as two-dimensional aerofoils, without interaction between the different elements of the blade. This way, radial velocity and three-dimensional effects are neglected. The following figure shows the usual representation of a blade element.

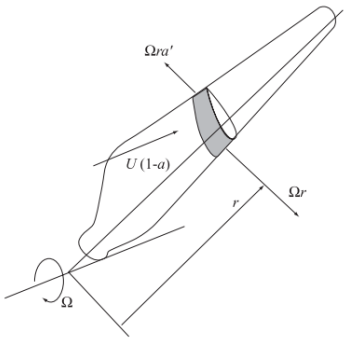

Figure 3: Blade element representation (Source:[7])

The cross section of a blade element, represented in 4, shows how the relative velocity at each blade segment depends on the rotor rotational velocity Ω, local radius r, pitch angle β, angle of attack α and induction factor a.

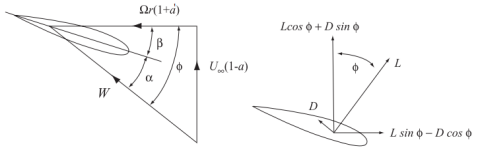

Figure 4: Blade element velocity and force vectors (Source: [7])

The relative flow velocity, as seen by the blade (making an angle ϕ relative to the plane of rotation), is given by:

$$W = \sqrt{U_\infty^2(1-a)^2 + \Omega^2 r^2(1+a')^2} \tag{8}$$

where the following relations can easily be obtained:

$$\tan\phi = \frac{U_\infty(1-a)}{\Omega r(1+a')} \quad , \tag{9}$$

$$\alpha = \phi - \beta \quad . \tag{10}$$

BEM Theory Results

By equating the thrust and the rate of momentum change from the element theory and momentum theory, respectively, the following expression for the axial induction factor is obtained:

$$a = \frac{1}{1 + \dfrac{4\sin^2\phi}{\sigma C_\mathrm{a}}}, \tag{11}$$

with $\sigma = cN_b/2\pi r$ being the rotor solidity and $C_\mathrm{a} = C_l \cos\ \phi + C_d \sin\ \phi$ being the non-dimensional component of force in the axial direction. The thrust coefficient is given by:

$$C_T = \frac{\sigma(1-a)^2 C_\mathrm{a}}{sin^2\phi}. \tag{12}$$

The tangential induction factor is given by:

$$a' = \frac{1}{-1 + \dfrac{4 \sin\ \phi \cos\ \phi}{\sigma C_\mathrm{r}}}, \tag{13}$$

with $C_\mathrm{r} = C_l \sin\ \phi + C_d\ \cos\ \phi$ being the non-dimensional component of force in the radial direction.

The original BEM model does not take into account several important effects that occur in reality, given its simplicity and assumptions made. Several corrections were developed in order to improve the model's reliability. The most common ones are the tip and hub loss, as well as Glauert's correction.

In 2005, Buhl came up with a modification for Glauert's original correction, to allow the model to be well represented for different correction factors, removing the discontinuity and the numerical instability present with Glauert's original correction.

Additionally, in the 1940's, while investigating propeller aerodynamics, Himmelskamp noticed that the lift force acting on rotating wings was larger than that of a non-rotating wing. The phenomenon, which also occurs in wind turbines is behind the need for the 3D Stall-Delay correction.

When performing BEM theory iterations, local angles of attack can oscillate and reach values outside normal operating range. These are the reasons why there is a need for a polar extrapolation procedure. Viterna-Corrigan extrapolation was the method implemented.

The implementation of the BEM theory iterative procedure follows Aerodyn's Theory Manual. Initially a first guess of the induction factors, a and a', is needed. With equations (9) and (11), and assuming that the inflow angle is small ($\sin(\phi) \approx \phi$), the tangential induction factor a' and drag coefficient C_d are both zero, the lift coefficient is given by $C_l = 2\pi\alpha$ and that the correction factors are equal to 1, the axial induction factor can be initially estimated to be:

$$a = \frac{1}{4}\left[2 + \pi\lambda_r\sigma - \sqrt{4 - 4\pi\lambda_r\sigma + \pi\lambda_r^2\sigma(8\theta + \pi\sigma)}\right], \tag{14}$$

where $\lambda_r = \Omega r/U_\infty$ is the local speed ratio.

Then, the following steps are performed iteratively for each blade section i until convergence is reached. Convergence is evaluated by analysing the residual defined as

$$\mathrm{Res} = \sum_{i=0}^{N_b} \left(a_i^{\mathrm{iter}} - a_i^{\mathrm{iter}-1}\right)^2, \tag{15}$$

where N_b is the number of blade sections considered, and iter is the iteration number.

1) Calculate the inflow angle with Eq. (9)[1]
2) Calculate the local angle of attack with Eq. (10)
3) Interpolate polar data in order to obtain the lift and drag coefficients, C_l and C_d
4) Calculate C_a and C_r
5) Calculate the correction factor $F = F_\mathrm{tip} \cdot F_\mathrm{hub}$
6) Calculate the thrust coefficient with Eq. (12)
7) Calculate the axial induction factor a, $a = \dfrac{1}{1 + \dfrac{4F\sin^2\phi}{\sigma C_\mathrm{a}}}$ or with $a = \dfrac{18F - 20 - 3\sqrt{C_T\,(50 - 36F) + 12F\,(3F - 4)}}{36F - 50}$, if $C_T > 0.96F$
8) Calculate the tangential induction factor a', $a' = \dfrac{1}{-1 + \dfrac{4F \sin\ \phi \cos\ \phi}{\sigma C_\mathrm{r}}}$
9) Repeat until convergence (Convergence considered when the Residual is smaller than 10^{-5})

BEM Theory Limitations

With this procedure, several parameters can be evaluated at different locations along the blade's span, which yield an approximation to the flow conditions on operating rotors.

Table 1: Different parameters evaluated by the BEM Theory model

Axial induction factor	a
Tangential induction factor	a'
Axial force coefficient	C_a
Radial force coefficient	C_r
Local angle of attack	α (rad)
Local inflow angle	ϕ (rad)

These limitation of the BEM model include, but are not limited to:

- Assumptions that rotor annuli rings can be considered independent between each other;

[1] The arctangent function *atan2* should be used preferably to account for the different quadrants

- Assumption of steady flow, uniform flow over the rotor plane;
- Lack of inclusion of wake rotation model;
- Lack of inclusion of aeroelastic considerations.

Together, these limitations, hinder the possibility of using this model to precisely and accurately simulate the complex aerodynamic behaviour of the flow around WTs blades, namely in unsteady state simulations and in flows with fluctuating conditions.

4. Software Description

This section presents a brief description of the different modules developed and implemented in C (programming language).

Two modules were developed. Module I was developed from root and Module II was reengineered to better fit wind turbine reality, being based on earlier work [8]. The two modules can be used independently, or together, depending on the objectives of the user. Module I can be used individually to determine the aerodynamic forces acting on a wind turbine blade at different azimuthal positions and to discretize a blade into panels, while Module II is used exclusively to predict noise, using Formulation 1A of Farassat. The program developed can then, call for Module I, in order to compute aerodynamic loading and mesh the blade, results which will be used in Module II, or skip Module I altogether, in which case the user has to specify a file containing aerodynamic forces and a file containing the blade discretization.

Module I: Aerodynamic Loading & Blade Surface Meshing

Integration of BEM with XFOIL

In order to obtain reliable aerodynamic data to be used in the noise estimation routine, there must be a joint use of the BEM theory and XFOIL©. This is due to the fact that the local inflow angle dictates the local angle of attack, as well as the relative velocity at the different locations along the blade. This means that the BEM iterative procedure must be used in order to determine the correct local angle of attack and Reynolds number.

However, the BEM routine needs the values of C_l and C_d (together with several other parameters used to define the blade) in order to determine the induction factor and the relative velocity of the flow. XFOIL© provides a platform that allows the automation of this procedure.

The results obtained with the BEM theory can then be used with XFOIL in order to estimate the aerodynamic forces. The logical flowchart is:

- Initial XFOIL routine used to obtain polar data for the profiles to be used;
- Apply 3D Stall-Delay corrections and extrapolate polars;
- Pass obtained results to BEM.
- Iterative procedure used to obtain the local induction factor, angle of attack and relative flow velocity;
- Write results to be used in XFOIL.
- Final XFOIL routine used to obtain aerodynamic loading data acting on a blade;

Some of the variables that can be obtained with BEM model were used to verify and validate the numerical implementation of this "*sub-module*" and are presented in table 1.

The discretization of the blade surface into panels is an important part of the computations to be performed before entering in the noise prediction module. Computationally, the blades are discretized using the following steps:

- For each section along the span of the blade, identify the airfoil profile used;
- For each section and airfoil used run XFOIL and repanel the airfoil for the number of points defined by the user in the file *"InputAirfoils.txt"*;
- Read the new airfoil profile file and store the non-dimensional data points that define it;
- Dimensionalize the airfoil with the chord of that section;
- Subtract an offset ($\bar{c_0}/4$, $\bar{c_0}$ being the chord from the first section) from the x coordinates of each file, so that each file has the x-axis starting from the $\bar{c_0}/4$ point;
- Rotate the profile by the twist angle around the pitch axis (which passes through the $\bar{c_0}/4$ point);
- Write the mesh file *"mesh_file.msh"*.

Fig. 5 shows an example of a wind turbine blade discretized into panels with the methodology explained above and implemented computationally.

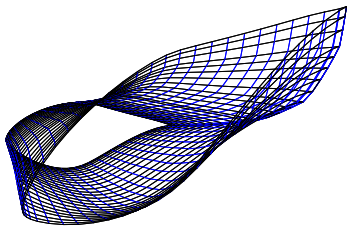

Figure 5: NREL's phase VI blade mesh

Module II: Noise Prediction

The first procedure performed by this computational module is to read the input files, either calculated previously by Module I or obtained externally by the user. Then, the Acoustic Simulation using Formulation 1A of Farassat, using a source time-dependent algorithm, follows the next procedure[2]:

- The blade is placed at a certain position in space (this position depends on the time-steps and rotational velocity);
- Calculate the velocity of the different blade panels and sections in the global system of coordinates;
- Calculate loading and thickness noise terms;
- Interpolate the calculated values of noise to the correct time instant, so the noise produced by different sources can be added together;
- Save the previous emission time and update the emission time.

The interpolation algorithm needs to ensure that the noise results are interpolated correctly to the right time instant, so that the noise produced by all sound sources, here considered to be either blade/wing surface panels or sections, can be added together. This involves saving the noise emitted by all the panels and sections from the previous emission time, for each emission time/ simulation step. Then, it is verified whether there is a position on the interpolation vector corresponding to an observer time instant, which is contained between the previous observer time and the actual observer time. If this condition is met, then the noise can be interpolated to that time instant and added in the respective position on the respective interpolated noise vector. Having the noise from both Loading and Thickness terms from Formulation 1A of Farassat in two interpolated noise vectors, obtaining the total noise is as straightforward as a sum of these two vectors, entry by entry.

5. Validation and Verification

Aerodynamic Module

The validation of the BEM module was done against some data regarding the NREL's (National Renewable Energy Laboratory) Phase VI turbine.

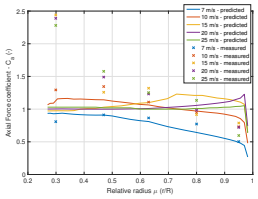

(a) Axial force coefficient

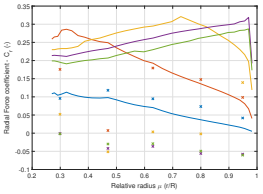

(b) Radial force coefficient

[2]This procedure is referent to each simulation time-step.

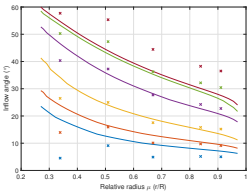

(c) Local inflow angle (same legend as Fig. 6(d))

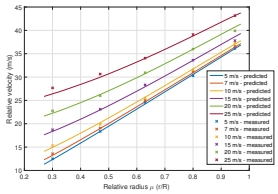

(d) Relative flow velocity

Figure 6: Comparison between BEM model and experimental results

The numerical tool selected as baseline for the verification of the BEM module developed was Aerodyn. This tool is publicly available (upon registration at NREL's web portal) and allows the obtainment of the aerodynamic response of a WT in the time-domain. The WT model used for the verification procedure is NREL's 5 MW reference WT, developed for offshore implantation and widely used academically for availability of design and operation specifications. The results obtained with the implemented BEM and with Aerodyn are presented in the next Figure (Figure 7). Here is presented the simpler case, with null tilt and yaw misalignment angles. Wind speed considered is 11.4 m/s.

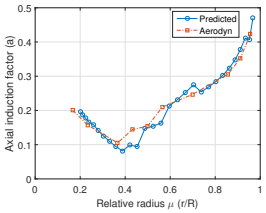

(a) Axial induction factor

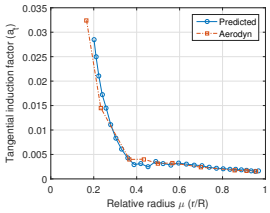

(b) Tangential induction factor

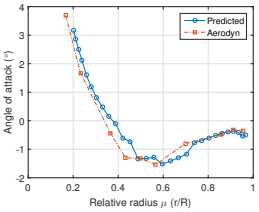

(c) Local angle of attack

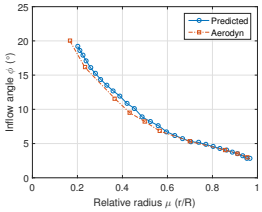

(d) Local inflow angle

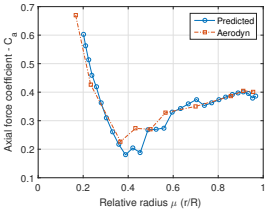

(e) Axial force coefficient

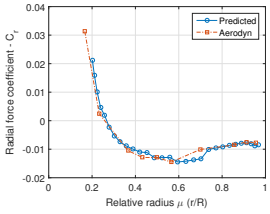

(f) Tangential force coefficient

Figure 7: Comparison between BEM model and Aerodyn results

The validation and verification of the BEM model implemented shows that it presents some limitations. The agreement between numerical results and experimental ones is not perfect, especially at very low and at higher flow velocities. The principal limitation of the model appears to be with increasing flow velocity. This is not entirely unexpected, since as the flow velocity increases so does the local inflow angle (see Fig. 6(c)) and the angle of attack ($\alpha = \phi - \beta$). As conditions are such that stall behaviour is encountered, the quality of the results obtained with XFOIL decreases considerably; Other causes for the error increase can be related with Viterna-Corrigan's extrapolation, that may not fully capture the behaviour after stall, and also the corrections implemented, namely the 3D-Stall delay correction, which difficultly is 100% accurate. However, for the usual range of wind speeds for which WTs are operating normally, the behaviour of the tested variables holds. Above 15 m/s of flow velocity the results deteriorate, but whenever wind speeds exceed this threshold the noise generated aerodynamically by the WT loses significance, since the noise begins to be dominated by background noise originated on the wind itself.

The verification procedure shows that results obtained with the implemented model agree well with the numerical results obtained with Aerodyn.

Aeroacoustics Module

Formulation 1A of Farassat - Test Case

In collaboration with TU Delft, both aerodynamic and noise data were shared for a simple case of a NACA 0018 profile in a wind tunnel. This airfoil was used to build a wing with a chord of 20cm and span of 40 cm, which was used during the experiments. Experiments were conducted at the Delft University of Technology vertical wind tunnel (V-Tunnel). The following figure follows with the frequency analysis in 1/3 octave bands of the two signals:

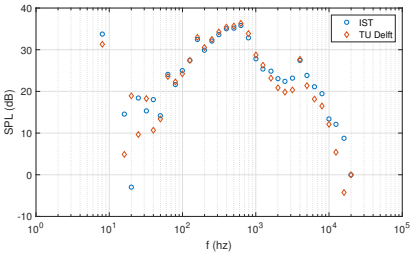

Figure 8: Frequency analysis in 1/3 octave bands

Results show an overall agreement. Frequencies between 10^2 Hz and 10^3 Hz are in close agreement. Discrepancies are most likely explained by differences in the numerical implementation of Formulation 1A, namely in the way that the time derivatives are calculated and how the total noise interpolation algorithm was developed. The implementation of Formulation 1A originates results which slightly overestimate noise at the lower and higher frequencies, when compared with results from TU Delft.

Semi-Empirical Models

The verification and validation of the implementation of semi-empirical noise models was performed using the Atlantic Orient Corporation (AOC) 15/50 wind turbine due to geometry and noise data availability.

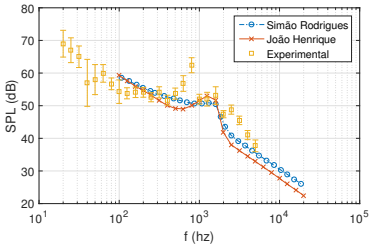

Figure 9: Noise generated by the AOC 15/50 wind turbine in 8 m/s winds

Comparison between aeroacoustic models

While not representative of a complete WT, the available data regarding the NACA 0018 wing can be used to compare the two aeroacoustic methodologies implemented. The following figure shows the results for the total noise obtained with the two methods.

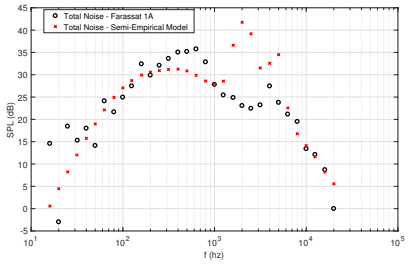

Figure 10: Comparison of aeroacoustic methods for the NACA 0018 wing with flow velocity of 20 m/s

Here, one can see that the two models attain similar results for frequencies below 1000 Hz and above 5000 Hz, with the overall shape of the curves agreeing. The removal of the Laminar Boundary Layer - Vortex Shedding Noise component from the semi-empirical formulation yields even better agreement [9].

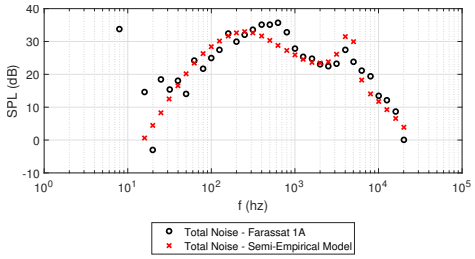

Figure 11: Comparison of Farassat 1A and Semi-empirical methods, without Laminar Boundary Layer - Vortex Shedding Noise component

Formulation 1A of Farassat is very interesting for allowing the attainment of a temporal variation of the acoustic pressure in most general cases, namely with a moving observer and/or moving bodies. It requires, however, detailed aerodynamic data, unsteady in nature and of complex obtainment. It remains at the state of the art when it comes to CAA methods.

The comparison between the two aeroacoustic methodologies, albeit for a simple case, shows that these agree. Even though the Laminar Boundary Layer - Vortex Shedding Noise component is included in Figures 10, appearing to have the largest contribution to the noise at around 2000 Hz, this contribution may not have the same impact in reality, since the flow was tripped in experimental set up (see [9]). At the same time, the results obtained with the Turbulent Inflow Noise present an overall agreement in terms of spectral shape, when compared to the results obtained with Formulation 1A. The peak at 4000 Hz is being correctly predicted by the Trailing Edge Bluntness Vortex Shedding Noise component.

Unfortunately, it was not possible to include in this document experimental acoustic results for this wing model, but one can expect those results to be somewhere along the lines of the results obtained with these two methodologies.

Semi-empirical methods are still commonly used in order to achieve a first approximation on the noise levels produced by wind turbines and in optimization problems, where the use of a more complex tool such as Formulation 1A would be too time consuming.

6. Prove of Software Aeroacoustic Capabilities

After extensive effort it become apparent that the objective of obtaining reliable aerodynamic and aeroacoustic data for a complete wind turbine rotor in operation, was presently out of reach. The principal difficulty came from the lack of readily available aerodynamic in conjunction with aeroacoustic data for complete wind turbine models, together with the challenging absence of associated geometric data for the wind turbine models for which there are aeroacoustic data available. Then, the difficulty in obtaining high resolution CFD data for the WTs for which there are the remaining data lead to the realization that there are still a couple of research topics on which to focus on future developments.

For these reasons, it was decided that an hypothetical scenario would be created, in order to demonstrate the aeroacoustic capabilities of the software designed, regarding formulation 1A of Farassat. For this, the aerodynamic data for the NACA 0018 profile, provided by TU Delft, were used to create a theoretical model of a wind turbine. An adaptation of NREL's 5 MW reference turbine was performed. This adaptation consisted in replacing the airfoils that this turbine uses for the airfoil NACA 0018, scaling the model with the chord of NREL's turbine and the aerodynamic data with the rotational velocity of this turbine at each section along the blade's span.

Obviously, this procedure has several shortcomings, but it serves to illustrate the capabilities of the designed software. The following figure presents the results obtained with such approach for three cases.

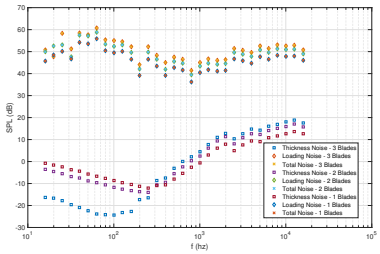

Figure 12: Hypothetical noise generated by the adapted NREL's wind turbine

The following table presents the OASPL for each of the simulations.

Table 2: Hypothetical scenarios OASPL

Scenario	OASPL (dB)
1 Blade	88.248
2 Blades	91.365
3 Blades / 12 rpm	93.110
3 Blades / 24 rpm	102.700
3 Blades / 48 rpm	114.066

As expected, OASPL increases with both the number of blades as well as with the rotational speed of the WT. The thickness noise has a very strong dependence on the rotational speed, as does the loading noise does. The loading noise, however, also has a strong dependence on the loads acting

on the surface of the blades, and since these change with the rotational speed, it is difficult to conclude exactly which is the strongest dependency.

Evidently, this procedure serves only to show the possibilities of using this software, when coupled with the appropriate input files. The theoretical aeroacoustic module is able to export the time-series of the pressure fluctuations in Pa, full power spectrum, as well as the 1/3 Octave Band analysis with OASPL, with the results presented in dBs and DBAs.

7. Conclusions

The objectives of this work were to develop a computational tool able to perform multiple tasks. The principal objective was the implementation of Formulation 1A of Farassat, in order to predict transient noise response of wind turbines.

The implementation of the wind turbine aerodynamic performance analysis module was validated against experimental data from NREL's Phase VI turbine and verified against Aerodyn©.

The implementation of the wind turbine aeroacoustic prediction module was: validated against experimental data from AOC's 15/50 turbine and verified against the implementation performed by Simão Rodrigues for his Master's Thesis [6], in the case of the semi-empirical models; and verified against the computational results obtained through a validated implementation of Formulation 1A of Farassat done by TU Delft, in the case of the theoretical model.

Achievements

The major achievements of the present work were:

- Development of a computational tool that can be used for the noise prediction of WTs;
- Development of a computational tool that can be used for the noise prediction of linear moving bodies, coupled with a panel surface discretization and aerodynamic pressure information as inputs;
- Development of a computational tool that can be used to predict the thickness and loading noise generated by a wind turbine rotor at any observer position;
- Development of a computational tool that can be used to predict the aerodynamic loadings acting on a wind turbine rotor;
- Development of a computational tool that can be used to discretize the blade geometry.

Future Work

During the work development for this dissertation, there were some issues that arose, and which would deserve to be addressed in future developments.

In summary, these are the points that would benefit from further research and that could improve the work developed:

- Inclusion of an expedite way to obtain unsteady aerodynamic wind turbine performance on the software;
- Inclusion of unsteady and aeroelastic models in the original BEM module, in order to allow the determination of accurate unsteady aerodynamic wind turbine response;
- Inclusion of more corrections in the BEM module;
- Evaluation of parametric impacts on noise results and computational cost;
- Development of a completely proprietary meshing software;
- Further improvements of the aerodynamic module, allowing different types of input from the end user.

References

[1] J E Ffowcs Williams and D L Hawkings. Sound Generation by Turbulence and Surfaces in Arbitrary Motion. *Philosophical Transactions of the Royal Society of London. Series A, Mathematical and Physical Sciences*, 264(1151):321–342, 1969.

[2] M J Lighthill. On Sound Generated Aerodynamically . I. *Proceedings of the Royal Society of London. Series A*, 211(1107):564–587, 1952.

[3] Renzo Tonin. Sources of wind turbine noise and sound propagation. *Acoustics Australia Journal*, 40(1):20–27, 2012.

[4] H H Hubbard, K P Shepherd, and P Shepherd. Wind turbine acoustics. *NASA Technical Paper*, 3057:20320–20377, 1990.

[5] F. Farassat and C. P. Succi. Review of Propeller Discrete Frequency Noise Prediction Technology With Emphasis on Two Current Methods for Time Domain Calculations. *Journal of Sound and Vibration*, 71(3):399–419, 1980.

[6] Simão Rodrigues. Aeroacoustic Optimization of Wind Turbine Blades. Master's thesis, Instituto Superior Técnico, Lisboa, Portugal, 2012.

[7] Tony Burton, David Sharpe, Nick Jenkins, and Ervin Bossanyi. *Wind Energy Handbook*. Number 1. 2001.

[8] Ana Elisa Vieira. Helicopter rotor noise : Development of an acoustic software tool. Master of science thesis, Instituto Superior Técnico, Lisboa, Portugal, November 2013.

[9] João Henrique Souto. Development of an aeroacoustic prediction tool for wind turbine noise. Master of science dissertation, Instituto Superior Técnico, Lisboa, Portugal, May 2017.